PERGAMON

Solid-State Electronics 45 (2001) 1821–1826

SOLID-STATE ELECTRONICS

Dynamic behavior of scaled microdisk lasers

S.M.K. Thiyagarajan, A.F.J. Levi *

Department of Electrical Engineering, University of Southern California, Denny Research, Building 118, Los Angeles, CA 90089-1111, USA

Received 2 March 2001; accepted 4 April 2001

Abstract

Room-temperature small-signal intensity-modulation frequency response of InGaAs/InGaAsP multiple quantum well microdisk lasers depends on disk radius. For frequencies up to 2 GHz the measured response of a small radius microdisk laser is closer to an ideal laser compared to larger devices. The dynamic response of larger radius lasers is strongly influenced by the presence of a reservoir of carriers in the non-lasing central portion of the disk. © 2001 Elsevier Science Ltd. All rights reserved.

1. Introduction

We report results of measuring the room-temperature small-signal modulation frequency response of InGaAs/InGaAsP multiple quantum well microdisk lasers. The response is found to depend on microdisk radius R because carriers in the non-lasing disk center are coupled to the lasing region via carrier diffusion.

Microdisk lasers combine the in-plane emission and ease of fabrication of conventional lasers with the key advantages of small device area and low threshold powers [1].

Although much research in the subject of microdisk lasers has been reported [2–11], very little is understood about their dynamic performance. Recently, Luo and co-workers measured impulse response of GaAs/AlGaAs microdisk lasers [12]. In their work, the microdisk was maintained at the low temperature of $T = 4$ K. In this work, we report results of measuring the dynamic response of optically pumped InGaAsP/InGaAs/InP microdisk lasers at room temperature [13].

2. Experiment

Light from a pump laser operating at an emission wavelength $\lambda_{\text{pump}} = 980$ nm is used to inject carriers into microdisk lasers. The microdisk lasers are fabricated using methods similar to those described previously [5]. To achieve continuous room-temperature operation, we use a multiple-quantum well InGaAsP semiconductor disk active gain medium wafer bonded to sapphire. Sapphire has a high thermal conductivity ($\kappa_{\text{sapphire}} = 0.43$ $\text{W cm}^{-1}\,\text{K}^{-1}$), low refractive index ($n_{\text{sapphire}} = 1.78$) and low optical loss. During wafer bonding, the semiconductor containing the epitaxially grown active region and sapphire are sandwiched between polished graphite discs. [1] The graphite discs are held together with molybdenum bolts. [2] At the wafer-fusion temperature of 400°C, the differential thermal expansion ($\alpha_{\text{graphite}} = 7.8 \times 10^{-6}$ K^{-1} and $\alpha_{\text{moly}} = 4.9 \times 10^{-6}$ K^{-1}) between graphite and molybdenum results in a compressive force between the sapphire and semiconductor during the wafer-fusion process.

Optical emission from the multiple quantum-well active region of a microdisk laser is collected perpendicular

* Corresponding author. Tel.: +1-213-740-7318; fax: +1-213-740-9280.

E-mail address: alevi@usc.edu (A.F.J. Levi).

[1] The graphite discs are machined from graphite purchased from Poco Graphite [14].

[2] The molybdenum bolts were obtained from Thermoshield [15].

PII: S0038-1101(01)00176-9

to the plane of the disk and substrate. Collected lasing intensity near wavelength $\lambda = 1550$ nm is amplified using a custom-built co-propagating two-stage erbium-doped fiber amplifier (EDFA) which provides high gain and low noise figure [16]. To improve signal-to-noise ratio, spontaneous emission from the EDFA is suppressed using a filter with a free spectral range of 56 nm and a -3 dB bandwidth of 10 GHz (0.08 nm). All measurements reported here are performed with the device at room temperature ($T = 300$ K). For the modulation experiments, incident pump power is varied sinusoidally at a frequency f according to $P_{ex}(t) = P_{bias} + (P_{mod} \times \sin(2\pi ft))$ by modulating current to the pump laser diode.

Fig. 1(a) shows measured collected lasing power P_{out} versus incident external pump power P_{ex} for a typical $R = 2.2$ μm radius microdisk. This specific device operates at a lasing wavelength, $\lambda_0 = 1554$ nm and $P_{th,ex} = 350$ μW. If one calibrates for the fraction of incident power absorbed by the semiconductor, the room-temperature lasing threshold occurs for absorbed pump power less than 175 μW. Inset to the figure shows lasing emission above threshold ($P_{ex} = 1.6 \times P_{th,ex} = 560$ μW) at wavelength $\lambda_0 = 1554$ nm.

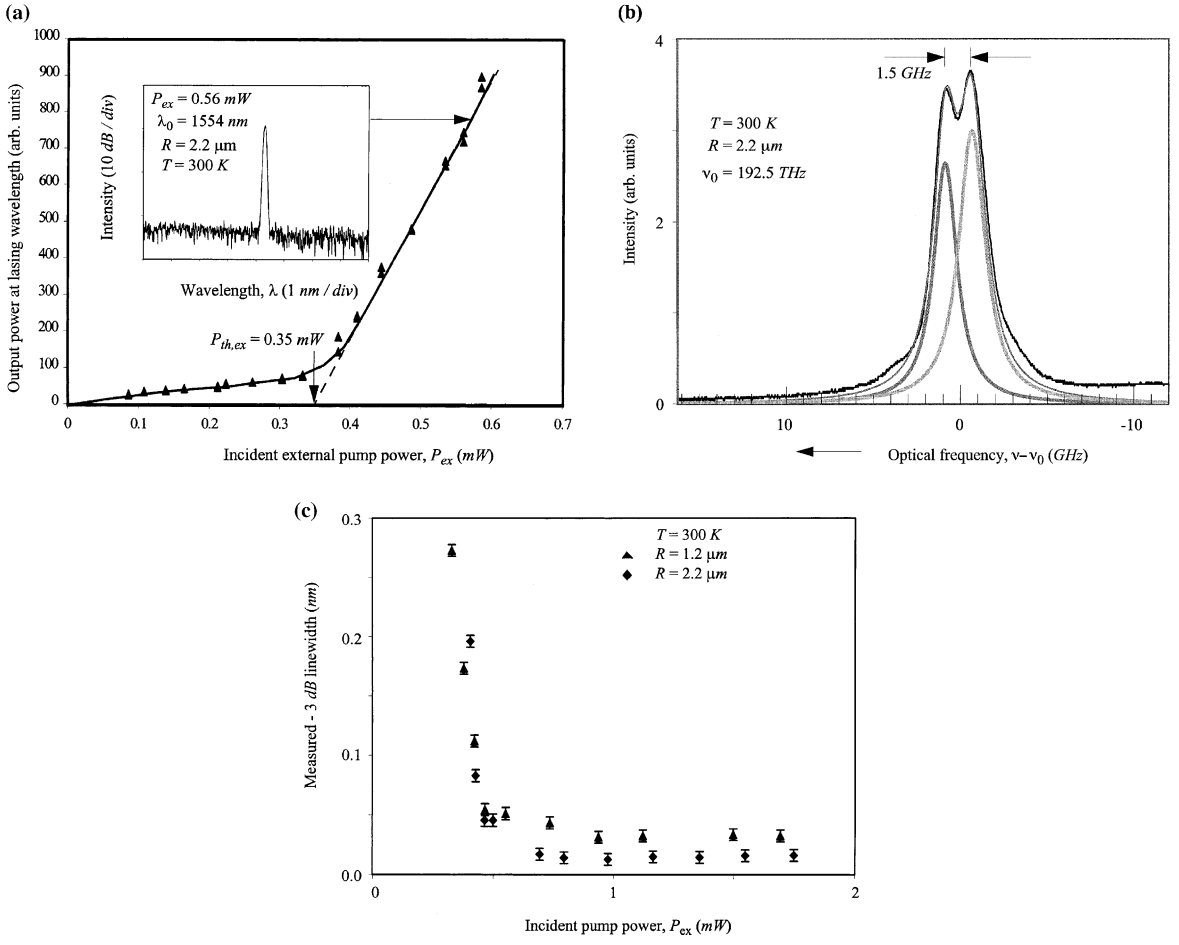

Fig. 1. (a) Measured optical power P_{out} at the lasing wavelength at room-temperature $T = 300$ K versus continuous external incident pump power P_{ex} at wavelength $\lambda_{pump} = 980$ nm for a radius $R = 2.2$ μm microdisk. Threshold pump power is $P_{th,ex} = 0.35$ mW. Inset shows measured room-temperature luminescence spectra at $P_{ex} = 1.6 \times P_{th,ex} = 0.56$ mW and lasing at wavelength $\lambda_0 = 1554$ nm. The line-width of the lasing resonance is limited by the 0.1 nm resolution of the spectrometer. The wavelength span is from $\lambda = 1550$ nm to $\lambda = 1558$ nm. (b) Measured line-shape of the lasing line at $\lambda_0 = 1558.3$ nm ($\nu_0 = 192.5$ THz) for a typical $R = 2.2$ μm radius microdisk at $P_{ex} = 2.76 \times P_{th,ex} = 1.16$ mW. The vertical and horizontal axis are linear scale. The presence of two very competing resonances spaced 0.012 nm (1.5 GHz) is clearly seen. The measured line-shape along with fit to measured data obtained using a sum of two Lorentzian line-shapes is shown. The individual Lorentzian line-shapes are also shown in the figure. (c) Measured room-temperature continuous-wave line-width of the dominant lasing resonance ($\delta\lambda$) versus incident external pump power P_{ex} for a disk with (i) $R = 1.2$ μm (triangles) and (ii) radius, $R = 2.2$ μm (rhombus). Threshold pump power for $R = 1.2$ μm and $R = 2.2$ μm device is $P_{th,ex} = 0.4$ mW.

Fig. 1(b) shows measured line-shape for a typical $R = 2.2$ μm microdisk with $P_{ex} = 2.8 \times P_{th,ex} = 1.16$ mW. Lineshape is measured using a scanning Fabry–Perot interferometer with a free spectral range of 150 GHz (1.2 nm) and a −3 dB bandwidth of 0.87 GHz (0.007 nm). Back-scattering from roughness at the microdisk periphery lifts degeneracy between clockwise and counterclockwise propagating whispering gallery resonances at ω_0 [17] and leads to two discrete standing-wave resonances at ω_- and ω_+. Devices with ω_- and ω_+ resonances split larger than 10 GHz have also been measured for devices with threshold pump powers greater than 1 mW. As shown in Fig. 1(b), the sum of two Lorentzian lineshapes is used to fit to the measured data and extract the linewidth of the dominant lasing resonance.

Fig. 1(c) shows the dependence of measured room-temperature line width of the dominant lasing resonance as a function of continuous incident external pump power for the indicated values of R. For a given R, the line width is found to decrease with increase in incident pump power until threshold is reached. At threshold, line width narrows significantly indicating onset of lasing. With further increase in pump power, no decrease in line width is observed and the measured line width saturates. The minimum value of line width is 0.013 nm (0.032 nm) or 1.6 GHz (3.9 GHz) for a $R = 2.2$ μm (1.2 μm) device. Previous measurement of microdisk laser emission line width [18] failed to observe the split ω_- and ω_+ resonances due to at least a factor of 10 inferior measurement resolution. The existence of the split ω_- and ω_+ resonances is important because of its impact on physical mechanisms determining laser emission line width and noise.

The response of the microdisk laser to small-signal intensity modulation is studied by modulating the input pump power at wavelength $\lambda_{pump} = 980$ nm. The measured small-signal intensity response −3 dB bandwidth of the pump light is 2.13 GHz (see Fig. 2(a)). This value, which includes detector response, is dominated by a 2.25 GHz detector bandwidth.

Fig. 2(b) shows the measured small-signal intensity modulation frequency response of a typical $R = 1.2$ μm microdisk laser at the indicated bias pump powers, $P_{bias,ex}$. An incident optical modulation power of amplitude $P_{mod} = 40$ μW is used. At incident pump power $P_{bias,ex} \leqslant P_{th,ex}$ carrier lifetime dominates small-signal intensity response and leads to conventional below-lasing-threshold behavior with a measured −3 dB bandwidth of 490 MHz for $P_{bias,ex} = P_{th,ex} = 0.26$ mW. However, at an incident pump power of $P_{bias,ex} = 1.3 \times P_{th,ex}$, the measured −3 dB bandwidth is 1.39 GHz and the small-signal intensity response does not show a relaxation oscillation peak.

Fig. 2(c) shows results of measuring small-signal intensity response of a typical $R = 2.4$ μm microdisk laser at the indicated bias pump powers, $P_{bias,ex}$. At an incident pump power $P_{bias,ex} = P_{th,ex} = 0.62$ mW carrier lifetime dominates small-signal intensity response and has a measured −3 dB bandwidth of 0.4 GHz. However, at an incident pump power of $P_{bias,ex} = 1.3 \times P_{th,ex}$, the measured −3 dB bandwidth is 1.7 GHz with a damped relaxation oscillation peak at 1.2 GHz. Unlike a conventional laser and a $R = 1.2$ μm microdisk laser, small-signal response of the $R = 2.4$ μm microdisk laser at $P_{bias,ex} = 1.3 \times P_{th,ex}$ exhibits a characteristic roll-off at frequencies up to 400 MHz.

We expect small-signal intensity response of a microdisk laser to be different from conventional lasers because the device consists of a lasing and non-lasing region coupled by carrier diffusion. Lasing into a whispering-gallery resonance occurs in a region localized within about 0.7 μm of the interior periphery of the disk. Hence, carrier recombination via stimulated emission occurs only near the edge of the microdisk. In the middle of the disk the device behaves similar to a light-emitting diode and carriers are not pinned above threshold (see inset to Fig. 3(a)). The two regions are coupled via carrier diffusion [19]. The characteristic roll-off at frequencies up to 400 MHz in the large $R = 2.4$ μm device of Fig. 2(c) is due to relatively weak coupling between carriers in the lasing and non-lasing regions. For a given diffusion coefficient, with decreasing R carriers in the middle of the disk are more strongly coupled to carriers at the disk edge. Hence, small-signal response of a microdisk laser behaves similar to a conventional laser for small R but differs significantly from a conventional laser for large R due to the presence of non-pinned carriers. Results of rate-equation modeling confirm this explanation of the observed behavior.

3. Numerical simulations

To better understand why device radius has such a dramatic influence on small-signal response, we study small-signal response of microdisk lasers using rate equations. We expect small-signal intensity response of a microdisk laser to be different from conventional lasers because a microdisk laser operates into a whispering-gallery resonance which is spatially confined to a region near the periphery of the disk. Hence, carrier recombination via stimulated emission occurs only near the edge of the microdisk (the lasing region) and not near the middle of the microdisk (which acts as a reservoir of carriers). This carrier reservoir region in the middle of the disk will be referred to as the light-emitting-diode-like (LED-like) region in the rest of this work (see inset to Fig. 3(a)). A second difference compared to a conventional laser arises due to possible spatial inhomogeneity of the pump beam and hence carrier inhomogeneity in the active region.

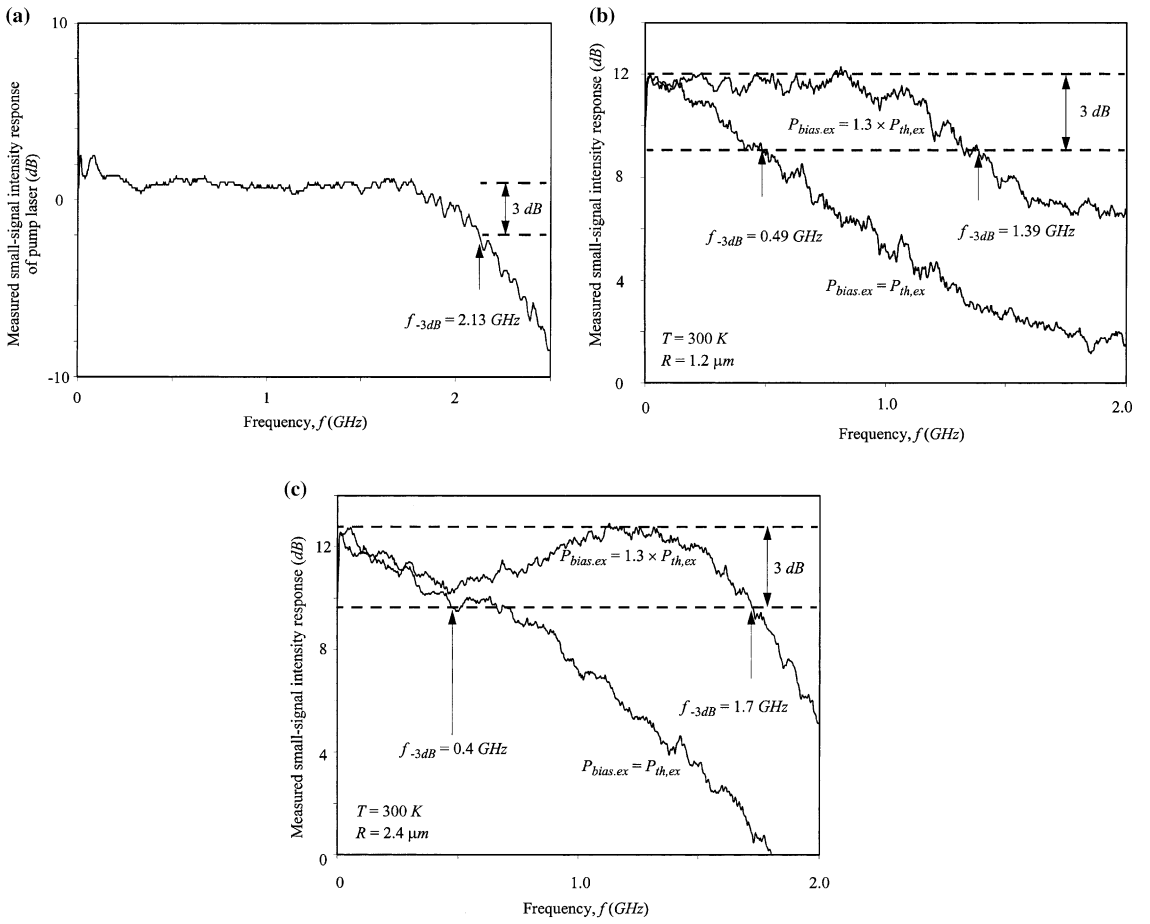

Fig. 2. (a) Measured small-signal intensity response for the pump laser used in our study. The threshold current for the pump laser is 14 mA. The device is biased at 21 mA and is modulated with a small signal of power equal to −20 dBm. The measured −3 dB response of 2.13 GHz is dominated by the 2.25 GHz bandwidth of the detector used. (b) Measured small-signal intensity response for a typical $R = 1.2$ μm microdisk at room temperature, $T = 300$ K for the indicated values of incident pump power bias $P_{\text{bias,ex}}$ and a modulation power of amplitude $P_{\text{mod}} = 40$ μW. When the microdisk laser is biased at threshold, $P_{\text{bias,ex}} = P_{\text{th,ex}} = 0.26$ mW, small-signal response is limited by carrier lifetime. The measured −3 dB bandwidth is 0.49 GHz. At $P_{\text{bias,ex}} = 1.3 \times P_{\text{th,ex}}$, the −3 dB bandwidth increases to 1.39 GHz with no observable relaxation oscillation peak. (c) Measured small-signal intensity response for a typical $R = 2.4$ μm microdisk at temperature $T = 300$ K for the indicated values of incident pump power bias $P_{\text{bias,ex}}$ and a modulation power of amplitude $P_{\text{mod}} = 20$ μW. At $P_{\text{bias,ex}} = P_{\text{th,ex}} = 0.62$ mW, small-signal response is dominated by the carrier lifetime. The measured −3 dB bandwidth is 0.4 GHz. At $P_{\text{bias,ex}} = 1.3 \times P_{\text{th,ex}}$, the −3 dB bandwidth increases to 1.7 GHz with a relaxation oscillation peak at 1.2 GHz. A roll-off in small-signal response is seen at low frequencies up to 0.4 GHz which is unique to large diameter microdisk lasers.

Accounting for carrier diffusion between the carrier reservoir in the middle of the disk and the carriers in the internal periphery of the disk, the device may be modeled as

$$\frac{dS}{dt} = (G - \kappa)S + \beta R_{\text{sp}} \tag{1}$$

$$\frac{dN_{\text{II}}}{dt} = \left(\frac{P_{\text{II}}}{h\nu}\right) - GS - \frac{N_{\text{II}}}{\tau_n(N_{\text{II}})} - D \times (N_{\text{II}} - N_{\text{I}}) \tag{2}$$

and

$$\frac{dN_{\text{I}}}{dt} = \left(\frac{P_{\text{I}}}{h\nu}\right) - \frac{N_{\text{I}}}{\tau_n(N_{\text{I}})} - D \times (N_{\text{I}} - N_{\text{II}}) \tag{3}$$

S and N_{II} are total photon and carrier (electron) numbers in the lasing cavity near the periphery of the microdisk, and N_{I} is the total number of carriers (electrons) in the middle of the disk. $P_{\text{II}}/h\nu$ ($P_{\text{I}}/h\nu$) is the carrier injection rate due to optical pumping in the laser region (LED-like region). $G(\kappa)$ is optical gain (loss), β is the fraction of total spontaneous emission that couples into the lasing mode. R_{sp} is spontaneous emission into all optical modes. We assume lasing in a single longitudinal

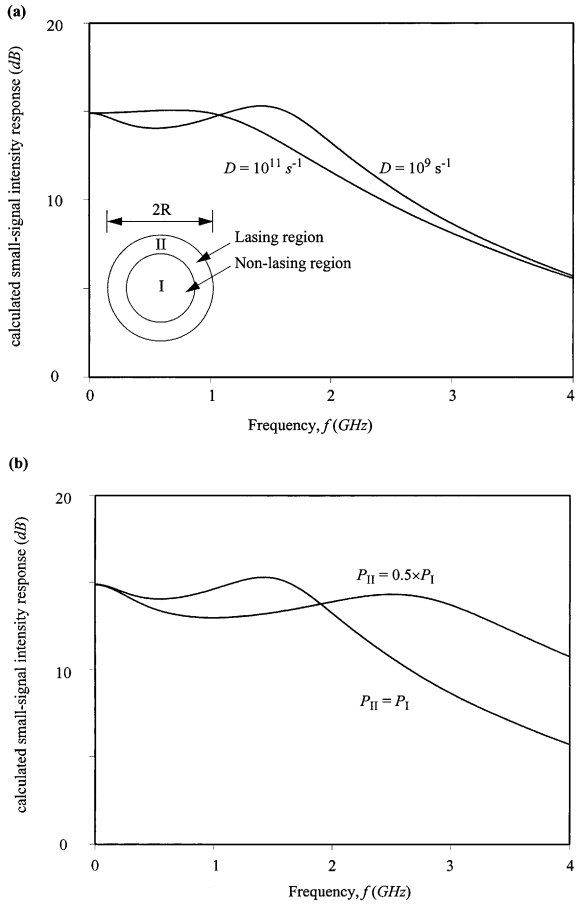

Fig. 3. (a) Calculated small-signal intensity response for a typical device of volume $V = 12.5 \times 10^{-4} \times 0.5 \times 10^{-4} \times 0.04 \times 10^{-4}$ cm^3 assuming uniform pump power across the microdisk. The device is biased at $P_{bias} = 1.3 \times P_{th} = 96$ μW and a modulation of 0.1 μW is applied. Inset shows a schematic illustration of the laser region and the LED-like region. (b) Calculated small-signal intensity response for a typical $V = 12.5 \times 10^{-4} \times 0.5 \times 10^{-4} \times 0.04 \times 10^{-4}$ cm^3 device with (i) uniform injection such that $P_{II} = P_I$ and (ii) with non-uniform injection such that $P_{II} = P_I/2$.

mode, linear optical gain $G = \Gamma g_{slope} v_g (N_1/V - n_0) \times (1 - \varepsilon S/V)$ with $g_{slope} = 2.5 \times 10^{-16}$ cm^2, optical transparency carrier density $n_0 = 1.0 \times 10^{18}$ cm^{-3}, optical mode confinement factor $\Gamma = 0.1$, photon group velocity $v_g = 7.5 \times 10^9$ cm s^{-1}, gain compression, $\varepsilon = 5 \times 10^{-18}$ cm^3 and active volume $V = 2.5 \times 10^{-13}$ cm^3. The 10 cm^{-1} internal loss and radiative recombination coefficient $B = 1 \times 10^{-10}$ cm^3 s^{-1} used in our study are typical of InGaAsP lasers [20]. Total optical loss $\kappa = 5.75 \times 10^{11}$ s^{-1} is used. Ignoring QED effects, $R_{sp} = BN_I^2/V$ is assumed. Carrier recombination rate $1/\tau_n(N) = (AN/V + BN^2/V^2)$ and non-radiative recombination rate $A = 1 \times 10^8$ s^{-1} is used. For the sake of simplicity, we assume that the active volumes of the LED-like region and the laser region are identical and also choose the lasing cavity to resemble a Fabry–Perot laser. The rate of diffusion D and β is 1×10^9 s^{-1} (since the carrier recombination rate is of order 1 ns) and 1×10^{-3} for a $R = 2$ μm device. To mimic the smaller radius device, we keep all other parameters fixed and increase D and β to 1×10^{11} s^{-1} and 4×10^{-3}. Since the radial carrier–density profile in the LED-like region is exponential and since the lasing resonance occupies a region ~0.7 μm near the internal periphery of the disk, two-orders of magnitude difference in the values of D can easily be achieved ($e^{(2-0.7)/(1-0.7)} = 76$) when the radius is decreased from 2 to 1 μm.

Fig. 3 shows the calculated small-signal intensity response for a $12.5 \times 10^{-4} \times 0.5 \times 10^{-4} \times 0.04 \times 10^{-4}$ cm^3 device assuming optical pump power is uniformly incident on the microdisk, i.e. $P_I = P_{II}$. Time dependence of the optical pump power is chosen to be of the form, $P_I(t) = P_{II}(t) = P_{bias} + (P_{mod} \times \sin(2\pi ft))$ where P_{bias} is the bias pump power, P_{mod} is the modulation amplitude and f is the modulation frequency. The device is biased at $P_{bias} = 1.3 \times P_{th} = 96$ μW and a modulation amplitude of 0.1 μW is applied. For $D = 1 \times 10^9$ s^{-1} the small-signal output modulation depth decreases with increase in frequency for frequencies < 500 MHz. Signal output then increases with increase in frequency up to the relaxation oscillation frequency before finally decreasing with further increase in frequency. This behavior is qualitatively similar to the measured results shown in Fig. 2(c) for a $R = 2$ μm device when biased at $P_{bias,ex} = 1.3 \times P_{th,ex}$. When $D = 1 \times 10^{11}$ s^{-1} and $\beta = 4 \times 10^{-3}$ (to simulate the effect of reducing the disk diameter), the modulation response is independent of frequency for low frequencies and decreases monotonically with increase in frequency at higher frequencies. The measured small-signal intensity modulation response for a $R =$ 1 μm device shown in Fig. 2(b) agrees qualitatively with the trends present in the model calculation.

Fig. 3(b) shows the effect of spatial inhomogeneity in pump power that excites carriers in the microdisk for a $D = 1 \times 10^{11}$ s^{-1} and $\beta = 4 \times 10^{-3}$ device. Comparing the case of $P_I = P_{II}$ with $P_I = 2 \times P_{II}$, we find that the relaxation oscillation peak becomes increasingly damped and the relaxation oscillation frequency increases with increase in inhomogeneity of pumping. The low frequency response also becomes increasingly LED-like when excitation is weighted towards the LED.

Our model can also be used to estimate turn-on delay and transient step response of the microdisk laser. Results of numerical simulation indicate that the dependence of turn-on delay, t_d on the low value of incident pump power, P_{low} is qualitatively similar to the measurements reported previously [13].

4. Conclusion and summary

In summary, microdisk lasers have a demonstrated high-speed modulation response in excess of 1.7 GHz when biased 1.3 times above threshold. The modulation frequency response spectrum is found to be strongly dependent on disk radius. This dependence is due to presence of a carrier reservoir in the middle of the disk. The measured line shape of lasing output indicates presence of two non-degenerate resonances. The estimated line width at room temperature for a $R = 1.2$ μm (2.2 μm) device biased just above threshold is 3.9 GHz (1.6 GHz).

Acknowledgements

This work is supported in part by CHIPS subcontract #10191574.

References

[1] Levi AFJ, McCall SL, Pearton SJ, Logan RA. Room temperature operation of submicrometre radius disk laser. Electron Lett 1993;29:1666–7.
[2] Ries MJ, Chen EI, Holonyak Jr N, Iovino GM, Minervini AD. Planar native-oxide-based AlGaAs–GaAs–InGaAs quantum well microdisk lasers. Appl Phys Lett 1996; 68:1540–2.
[3] Corbett B, Justice J, Considine L, Walsh S, Kelly WM. Low-threshold lasing in novel microdisk geometries. IEEE Photon Tech Lett 1996;8:855–7.
[4] Bi WG, Ma Y, Zhang JP, Wang LW, Ho ST. Improved high-temperature performance of 1.3–1.5 μm InNAsP–InGaAsP quantum-well microdisk lasers. IEEE Photon Technol Lett 1997;9:1072–4.
[5] Thiyagarajan SMK, Levi AFJ, Lin CK, Kim I, Dapkus PD, Pearton SJ. Continuous room-temperature operation of optically pumped InGaAs/InGaAsP microdisk lasers. Electron Lett 1998;34:2333–4.
[6] Thiyagarajan SMK, Cohen DA, Levi AFJ, Ryu S, Li R, Dapkus PD. Continuous room-temperature operation of microdisk laser diodes. Electron Lett 1999;35:1252.
[7] Fujita M, Inoshita K, Baba T. Room temperature continuous wave lasing characteristics of GaInAsP/InP microdisk injection laser. Electron Lett 1998;34:278–9.
[8] Thiyagarajan SMK, Levi AFJ. Active microdisk devices. Proceedings of SPIE 2000, San Jose, CA, USA, vol. 3947; 2000. p. 185–96. ISSN # 0277-786X.
[9] Levi AFJ, Slusher RE, McCall SL, Glass JL, Pearton SJ, Logan RA. Directional light coupling from microdisk lasers. Appl Phys Lett 1993;62:561–3.
[10] Backes SA, Cleaver JRA, Heberle AP, Koehler K. Microdisk laser structures for mode control and directional emission. J Vac Sci Technol B 1998;16:3817–20.
[11] Chu DY, Chin MK, Bi WG, Hou HQ, Tu CW, Ho ST. Double-disk structure for output coupling microdisk lasers. Appl Phys Lett 1994;65:3167–9.
[12] Luo KJ, Xu JY, Cao H, Ma Y, Chang SH, Ho ST, Solomon GS. Dynamics of GaAs/AlGaAs microdisk lasers. Appl Phys Lett 2000;77:2304–6.
[13] Thiyagarajan SMK, Levi AFJ. High-speed response of optically pumped InGaAs/InGaAsP microdisk lasers. Electron Lett 2001;37:175–6.
[14] Poco Graphite Inc., http://www.poco.com.
[15] Thermoshield, Los Altos, CA ((650) 941-5230).
[16] Becker PC, Olsson NA, Simpson JR. Erbium-doped fiber amplifiers. San Diego, CA: Academic press; 1999 [chapter 8].
[17] Weiss DS, Sangodhar V, Hare J, Lefèvre-Seguin V, Raimond JM, Haroche S. Splitting of high-Q Mie modes induced by light backscattering in silica microspheres. Opt Lett 1995;20:1835–7.
[18] Mohideen U, Slusher RE, Jahnke F, Koch SW. Semiconductor microlaser linewidths. Phys Rev Lett 1994;73:1785–8.
[19] Fujita M, Sakai A, Baba T. Ultrasmall and ultralow threshold GaInAsP–InP microdisk injection lasers: design, fabrication, lasing characteristics, and spontaneous emission factor. IEEE J Quant Electron 1999;58:673–81.
[20] Agrawal GP, Dutta NK. Semiconductor lasers, second edition. New York: Van Nostrand Reinhold; 1993 [chapter 6].